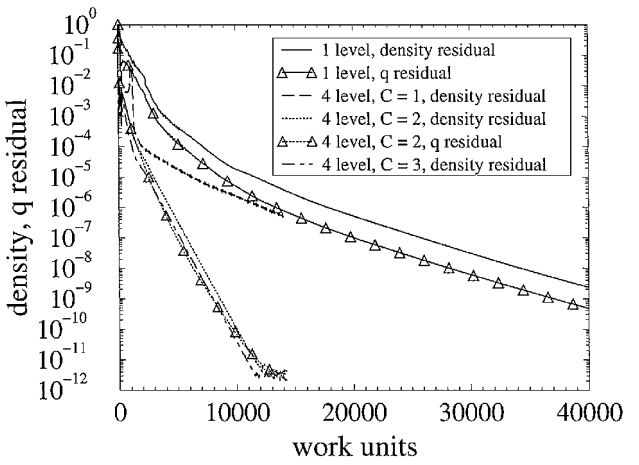

Fig. 4 Convergence history for density and turbulence residuals.

Conclusions

Some modifications for the restriction and prolongation process of multigrid methods have been presented that are necessary for the simulation of complex supersonic flowfields. Damping of the restricted residual error and blending between a second-order central and a first-order upwind prolongation enable convergence in supersonic flows and resulted in strong reductions in CPU time. The advantage of this kind of blending is the reduction to first-order prolongation at shock waves only.

Acknowledgments

We wish to thank the Deutsche Forschungsgemeinschaft for financial support of this work within the Collaborative Research Center SFB 259 at the University of Stuttgart.

References

[1]Turkel, E., Swanson, R. C., Vatsa, V. N., and White, V. N., "Multigrid for Hypersonic Viscous Two- and Three-Dimensional Flow," Inst. for Computer Applications in Science and Engineering, ICASE Rept. 91-57, Contract NAS1-18605, Hampton, VA, July 1991.

[2]Vatsa, V. N., Turkel, E., and Abolhassani, J. S., "Extension of Multigrid Methodology to Supersonic/Hypersonic 3-D Viscous Flows," *International Journal for Numerical Methods in Fluids*, Vol. 17, No. 10, 1993, pp. 825–837.

[3]Radespiel, R., and Swanson, R. C., "Progress with Multigrid Schemes for Hypersonic Flow Problems," *Journal of Computational Physics*, Vol. 116, Jan. 1995, pp. 103–122.

[4]Edwards, J. R., "Development of an Upwind Relaxation Multigrid Method for Computing Three-Dimensional Viscous Internal Flows," AIAA Paper 95-0208, Jan. 1995.

[5]Liu, F., and Shanhong, J., "Unsteady Flow Calculations with a Multigrid Navier–Stokes Method," *AIAA Journal*, Vol. 34, No. 10, 1996, pp. 2047–2053.

[6]Gerlinger, P., and Brüggemann, D., "Multigrid Convergence Acceleration for Turbulent Supersonic Flows," *International Journal for Numerical Methods in Fluids*, Vol. 24, No. 10, 1997, pp. 1019–1035.

[7]Gerlinger, P., and Brüggemann, D., "An Implicit Multigrid Scheme for the Compressible Navier–Stokes Equations with Low-Reynolds-Number Turbulence Closure," *Journal of Fluids Engineering*, Vol. 120, June 1998, pp. 257–262.

[8]Koren, B., and Hemker, P. W., "Damped, Direction-Dependent Multigrid for Hypersonic Flow Computations," *Applied Numerical Mathematics*, Vol. 7, April 1991, pp. 309–328.

[9]Leclercq, M. P., and Stoufflet, B., "Characteristic Multigrid Method to Solve the Euler Equations with Unstructured and Nested Grids," *Journal of Computational Physics*, Vol. 104, Feb. 1993, pp. 329–346.

[10]Jameson, A., and Yoon, S., "Lower–Upper Implicit Schemes with Multiple Grids for the Euler Equations," *AIAA Journal*, Vol. 25, No. 7, 1987, pp. 929–935.

[11]Swanson, R. C., and Turkel, E., "On Central Difference and Upwind Schemes," *Journal of Computational Physics*, Vol. 101, Aug. 1992, pp. 292–306.

[12]Gerlinger, P., Kasal, P., Boltz, J., and Brüggemann, D., "Numerical Investigation of Hydrogen Strut Injections into Supersonic Air Flows," AIAA Paper 98-3424, July 1998.

D. S. McRae
Associate Editor

Elliptic Grid Generation

Reijo Lehtimäki*
Helsinki University of Technology,
FIN-02015 HUT, Espoo, Finland

Introduction

GRID generation is an essential part of computational fluid dynamics. Structured multiblock grids can already in practice be generated into remarkably complex geometries. Grid generation is, however, a task that demands a major share of the man hours spent on the flow solution and that remains a research subject of practical interest.

In the two-dimensional case, the harmonic map is a diffeomorphism. Unfortunately, it seems this result cannot be generalized to three space dimensions.[1] Furthermore, the theorems are for the continuous map, and it is the discrete approximation that forms the grid. Yet the harmonic method is in practice very robust. Unfortunately, a straightforward application of the Laplace–Beltrami equation does not allow any control of the grid, but the grid always becomes evenly spaced in the interior. A common approach is to add an inhomogeneous term to the equation and to use this inhomogeneous equation, the Poisson equation, for grid generation.[2] One technique for calculating the control terms is to apply an intermediate parameter domain.[3] There are a number of other techniques as well, in which the Poisson system is applied without any concern about the regularity of the parameter domain to which the control terms possibly correspond. Methods based on the Beltrami equation directly, without any control terms, have also been developed. For example, Dvinsky applies predefined metrics in the physical domain to achieve grid control.[4]

In the present method, grid clustering is achieved via a clustered computational domain from which nonuniform difference increments are calculated in the discretization of the Laplace equation. The method does not include grid orthogonalization. The generated grid can be orthogonalized to the boundary afterward.[5] In fact, any orthogonalization requirements would make the grid-generation problem overdetermined.[5] Thus, adding an orthogonalization feature to the method, e.g., by adjusting the computational domain further, would probably lessen the robustness of the method.

Grid-Generation Equations

Harmonic maps are extremals of the energy functional. Consider a harmonic map from the physical to the computational domain. Suppose the computational space is a Euclidean space equipped with a Cartesian coordinate system ξ^n. If the physical space is also a Euclidean space and the coordinate system x^n Cartesian, then the Euler equation for the energy functional reduces to the Laplace equation. In the case of a nonvanishing Jacobian, the Laplace equation can be transformed so that the curvilinear coordinates appear as independent variables and the Cartesian coordinates as dependent[2]:

$$g^{kj}\frac{\partial^2 x^\lambda}{\partial\xi^k\partial\xi^j} = 0 \tag{1}$$

Here the g^{kj} are the contravariant components of the metric tensor of the coordinate system on the physical space induced by the harmonic map. Equation (1) is the grid-generation equation for two- and three-dimensional flat domains.

If the physical space is a curved surface in a three-dimensional Euclidean space, the application of the formulas of Gauss yields the harmonic grid-generation equation on a surface[2,6]:

$$g^{kj}\frac{\partial^2 x^\lambda}{\partial\xi^k\partial\xi^j} = G(K_1 + K_2)n^\lambda \tag{2}$$

Received Nov. 26, 1997; revision received Jan. 25, 1999; accepted for publication Jan. 29, 1999.

*Research Scientist, Laboratory of Aerodynamics, P.O. Box 4400.

where K_1 and K_2 are the principal curvatures of the surface, n^λ are the Cartesian components of the local unit normal vector, and G is the determinant of the covariant components of the metric tensor on the surface.

Discretization

A natural way to cluster the grid is to allow the boundary point distribution to carry into the field in the grid-generation process. To this end, a clustered computational domain is applied. The method is described here in the two-dimensional case. The extension to three space dimensions is straightforward.

Consider a harmonic map mapping a physical domain to a computational domain. The physical domain is assumed to have a predetermined uneven point distribution on the boundary. Consider then an even boundary point distribution on the same continuum boundary of the physical domain as the original uneven distribution. One way to illustrate the map is to draw ξ, e.g., as a function of x and y (Fig. 1). The values of ξ form a surface above the physical domain ascending from the grid line of $\xi = \xi_{\min}$ to the grid line of $\xi = \xi_{\max}$. Because of the maximum principle, this surface has no local minima or maxima in the interior. In the even-spaced harmonic grid, the grid lines of constant ξ are projections of the intersections of the surface with horizontal planes (Fig. 1). Suppose the surface is cut with nonhorizontal planes instead that match the predetermined points on the boundaries. Different grid lines from the same continuous solution are then obtained. For this purpose the computational space is discretized nonuniformly, as in Fig. 2 (left). The relative point distribution on the boundary of this computational domain is copied from the relative boundary point distribution of the physical domain, and the interior is interpolated.[7] This grid is then used to form nonuniform difference approximations for the derivatives in Eqs. (1) and (2). Thus, for example, the partial derivative $\partial x/\partial \xi$ is approximated by the second-order accurate difference approximation

$$\left(\frac{\partial x}{\partial \xi}\right)_{i,j} \approx \frac{\left(h^-_{i,j}\right)^2 x_{i+1,j} + \left[\left(h^+_{i,j}\right)^2 - \left(h^-_{i,j}\right)^2\right] x_{i,j} - \left(h^+_{i,j}\right)^2 x_{i-1,j}}{\left(h^-_{i,j}\right)^2 h^+_{i,j} + \left(h^+_{i,j}\right)^2 h^-_{i,j}} \tag{3}$$

Here the $h^+_{i,j}$ and $h^-_{i,j}$ are the forward and backward difference increments calculated from the clustered computational domain as

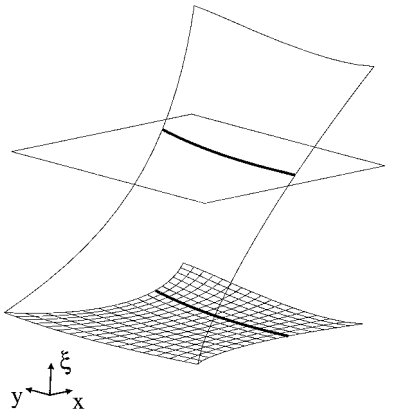

Fig. 1 Curvilinear coordinate ξ as a function of the Cartesian coordinates x and y. A coordinate line of constant ξ is the projection of the intersection of the ξ surface and a horizontal plane.

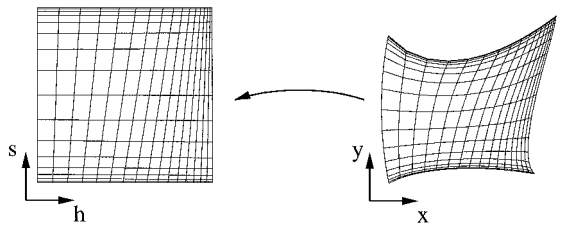

Fig. 2 Map from the physical domain to the computational domain.

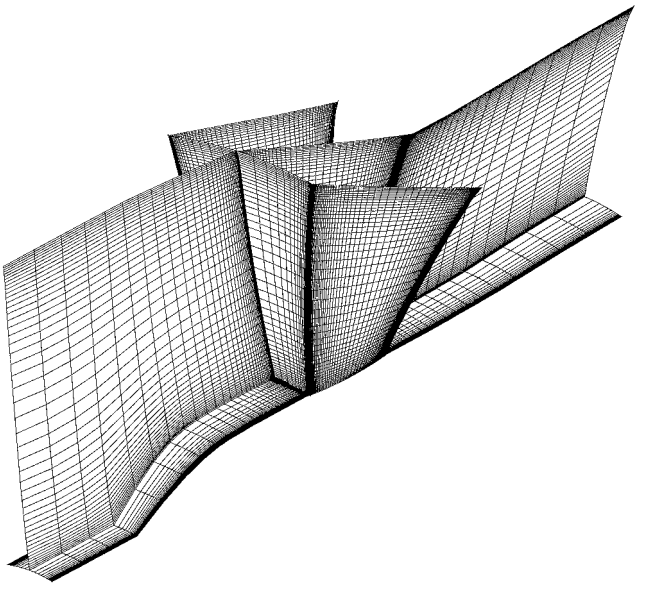

Fig. 3 Hub, blades, a coordinate surface passing through the blade passage in the middle, and the coordinate surface connecting the leading edges of the blades of the NASA 55C fan rotor grid.

$h^+_{i,j} = h_{i+1,j} - h_{i,j}$ and $h^-_{i,j} = h_{i,j} - h_{i-1,j}$. The clustering of the resulting grid in the physical domain then follows the clustering of the nonuniform grid in the computational domain (Fig. 2). Equations (1) and (2) are solved iteratively with the successive overrelaxation (SOR) method, lagging the metric coefficients. Unfortunately, when cutting the surface in Fig. 1 with nonhorizontal planes, the maximum principle, which operates vertically, does not guarantee a unique preimage for each point of the image. In fact, although the map satisfies the Laplace–Beltrami equation, it is not harmonic (to the clustered computational domain) because the Christoffel symbols on the image do not vanish, and the Laplace–Beltrami equation is no longer the Euler equation for the energy functional.

Grid Example

In Fig. 3, a $64 \times 48 \times 128$ cell grid for the NASA 55C fan rotor is shown. The numbers correspond to the circumferential, radial, and axial directions, respectively. The rotor has 15 blades, and because of the axial symmetry, only one blade passage is modeled. The surface grid-generation method is applied on the rotor hub, and the volume grid is generated with the three-dimensional method. The volume grid is depicted in the coordinate surface cutting the blade passage in the middle and in the cross section connecting the leading edges of the blades.

Conclusions

A method for the generation of computational grids based on the Laplace–Beltrami equation is presented. Grid clustering is achieved via nonuniform difference approximations. The difference increments are obtained from a clustered computational domain interpolated from the boundary point distribution. Thus, unlike in the straightforward application of the Laplace equation, in the present method the point distribution of the boundary carries over the field.

References

[1] Liao, G., Pan, T., and Su, J., "Numerical Grid Generator Based on Moser's Deformation Method," *Numerical Methods for Partial Differential Equations*, Vol. 10, No. 1, 1994, pp. 21–31.

[2] Thompson, J. F., Warsi, Z. U. A., and Mastin, C. W., *Numerical Grid Generation: Foundations and Applications*, North-Holland, Amsterdam, 1985, Chap. 6.

[3] Spekreijse, S. P., "Elliptic Grid Generation Based on Laplace Equations and Algebraic Transformations," *Journal of Computational Physics*, Vol. 118, No. 1, 1995, pp. 38–61.

[4] Dvinsky, A., "Harmonic Maps in Grid Generation," *Mathematical Aspects of Numerical Grid Generation*, edited by J. E. Castillo, Society for Industrial and Applied Mathematics, Philadelphia, PA, 1991, pp. 105–121.

[5] Lehtimäki, R., "A Simple Algebraic Grid Orthogonalization Procedure with Regularity Control," *Computational Fluid Dynamics '98. Proceedings*

of the Fourth European Computational Fluid Dynamics Conference, edited by K. D. Papailiou, D. Tsahalis, J. Périaux, and M. Pandolfi, Vol. 1, Wiley, New York, 1998, pp. 14–19.

[6]Warsi, Z. U. A., "Numerical Grid Generation in Arbitrary Surfaces Through a Second-Order Differential-Geometric Model," *Journal of Computational Physics*, Vol. 64, No. 1, 1986, pp. 82–96.

[7]Lehtimäki, R., "Grid Deformation Tools for Simulation of Free Surface Flows," *6th International Conference on Numerical Grid Generation in Computational Field Simulations*, edited by M. Cross, P. Eiseman, J. Häuser, B. K. Soni, and J. F. Thompson, International Society of Grid Generation, Mississippi State, MS, 1998, pp. 599–608.

J. Kallinderis
Associate Editor

Evaluation of Renormalization Group Turbulence Models for Dynamic Stall Simulation

Yang-Yao Niu*
Chung-Hua University,
Hsin-Chu 30067, Taiwan, Republic of China

Introduction

UNSTEADY stall phenomena are the result of airfoils and wings oscillating in pitch and having a maximum angle of attack greater than the static stall angle. The causes of this delay of stall, often accompanied with hysteresis in lift and moment coefficients, have challenged aerodynamicists for many years. As noted in the extensive studies by McCroskey[1] and McCroskey et al.,[2] the nonequilibrium nature of the separated turbulent boundary layer and the associated unsteady time-lag features are more difficult to analyze. Therefore an accurate turbulence model is required. In the evaluation of the turbulence models on dynamic stall, the renormalization group theory (RNG) algebriac model has demonstrated the efficiency and reasonable accuracy of the work of Srinivasan et al.[3] In the previous work,[4] the family of advection upwind splitting method (AUSM) schemes, together with the RNG-based algebraic model, is used for several steady-state and oscillating NACA 0012 airfoil flows. It was shown that AUSMD with a weighting function based solely on the density was robust and stable for the problem considered. Whereas in the light stall case numerical estimation of unsteady airload hysteresis was satisfactory, the deep dynamic stall case was not predicted successfully by the RNG-based algebraic model used. To continue this effort, two RNG-based algebraic models[5,6] and one RNG-based k-ϵ model[7] are selected for the present investigation of the deep stall case. Numerical results of one deep stall case of the NACA 0012 airfoil are compared with the experimental results of McCroskey et al.[2]

Numerical Models

The two-dimensional, Reynolds-averaged, Navier–Stokes equations with the kinetic energy and dissipation equations are written as

$$\frac{\partial \boldsymbol{Q}}{\partial t} + \frac{\partial \boldsymbol{F}}{\partial x} + \frac{\partial \boldsymbol{G}}{\partial y} = \left(\frac{\partial \boldsymbol{F}_v}{\partial x} + \frac{\partial \boldsymbol{G}_v}{\partial y}\right) + S \tag{1}$$

where x, y, and t are the Cartesian coordinates and time, $\boldsymbol{Q}$ the vector of the dependent variables, and $\boldsymbol{F}$ and $\boldsymbol{G}$ convective flux vectors. Also, the viscous flux vectors are represented by $\boldsymbol{F}_v$ and $\boldsymbol{G}_v$. In the implementation of the algebraic turbulence model, the kinetic energy and turbulence dissipation equations are not considered and the source term S is neglected. The governing equations are integrated with a dual-time-stepping procedure and discretized in the finite volume formulation with the AUSMD scheme. A second-order-accurate, three-point backward differencing is implemented for the physical time discretization, and a four-stage explicit Runge–Kutta scheme is implemented for the pseudotime evolution of solutions between the physical times.

RNG Turbulence Models

In the first RNG-based algebraic turbulence model, the eddy viscosity is expressed in the following formula:

$$\nu = \nu_t + \nu_l = \nu_l\left[1 + H\left(\frac{0.0192}{\nu_l^3}\epsilon L^{-4} - C\right)\right]^{\frac{1}{3}} \tag{2}$$

where the subscripts l and t refer to the laminar viscosity and turbulent viscosity, respectively; $C = \mathcal{O}(100)$ is the RNG constant; and H is the Heaviside step function. The length scale L is evaluated as

$$L = \frac{1}{y} + \frac{1}{0.225\delta} \tag{3}$$

The thickness parameter δ is defined as $\delta = 1.2y_{1/2}$ (Ref. 5), where $y_{1/2}$ is the normal distance from the wall at which the vorticity function attains its half-amplitude. The near-wall turbulence is reduced by implementing a dissipation rate ϵ:

$$\epsilon = \frac{2.5u_\tau^3}{y}\left[1 - \exp\left(-\frac{0.04\rho u_\tau y}{\mu_l}\right)\right] \tag{4}$$

where u_τ is the friction velocity.

In the so-called RNG algebraic Q4 model,[6] the eddy viscosity equation is obtained from a quartic equation:

$$Q_4(\nu) = \nu^4 + (C-1)\nu_l^3\nu - (\kappa^2\Omega\ell^2)^4 = 0 \tag{5}$$

where $C = \mathcal{O}(100)$ is the constant, κ the von Kármán constant, and Ω the vorticity function. This quartic equation has only one physically plausible root and is solved under the constraint $\nu = \max(\nu, \nu_l)$. In the determination of the length scale appearing in the quartic equation, $L = \min(y, \gamma y_{\max})$ is used by means of the normal distance $y_{\max}$ and the intermittency coefficient γ.

The RNG-based k-ϵ model[7] is also considered. An extra term R in the source term is required:

$$R = \frac{C_u\eta^3(1-\eta/\eta_0)}{1+\beta\eta^3}\frac{\epsilon^2}{k} \tag{6}$$

where $\eta = wk/\epsilon$, w is the magnitude of the rate of strain, and $C_u = 0.0845$.

The eddy viscosity is given by

$$\nu_t = \nu_l\left\{1 + \left[\left(\sqrt{C_u/\nu_l}\right)\left(k/\sqrt{\epsilon}\right)\right]\right\}^2 - \nu_l \tag{7}$$

Results

Two separated-flow cases of the NACA 0015 airfoil at high angles of attack are selected to evaluate the RNG turbulence models. The relevant parameters are $M_\infty = 0.3$, $Re_\infty = 3 \times 10^6$, and $\alpha = 13$ and 17 deg, the conditions reported in Ref. 4. Figure 1 compares the pressure coefficients from the computed and experimental results. In the mildly separated case ($\alpha = 13$ deg), the RNG-based algebraic model and the Q4 model give consistent surface pressure distributions that are also in close agreement with the data. However, the RNG k-ϵ model shows excessive numerical dissipation by smearing out the pressure coefficient distribution around the leading edge of the airfoil. In the strongly separated case ($\alpha = 17$ deg), the RNG model with the damping dissipation rate [Eq. (4)] gives a more reasonable prediction of the quasi-unsteady surface pressures than the other two RNG models. It is seen that the overall pressure coefficients are underpredicted by the RNG k-ϵ model but also additional computation cost is incurred. Among the selected RNG turbulence models, the RNG algebraic model with the damping dissipation function is shown to be the most cost effective in providing accurate solutions to the steady- and quasi-unsteady-statetest cases.

Received May 1, 1998; revision received Jan. 21, 1999; accepted for publication Jan. 29, 1999.

*Associate Professor, Department of Mechanical Engineering. Member AIAA.